Vacuum Polarization Solver

Pedro Carneiro

GoLP/Instituto de Plasmas e Fusão Nuclear, Instituto Superior Técnico, Universidade de Lisboa, 1049-001 Lisbon, Portugal

Abstract

In this work we address the quantum dynamics of the vacuum using a semi-classical theory developed by Heisenberg-Euler, treating the vacuum as an effective nonlinear medium by correcting the classical Maxwell's equations with a polarisation and magnetisation of the vacuum. We present the result of the main objective of this thesis: the development of a new numerical method to solve the set of Maxwell-Heisenberg-Euler equations, for the first time, in multi-dimensions. Our multidimensional solver reproduced, in one dimensional configurations, the results for which an analytic treatment is possible, yielding vacuum harmonic generation and birefringence. The accuracy of the code is demonstrated in 2D with simulations of the interaction between two Gaussian pulses, with realistic parameters, generating the respective high harmonics. Finally, we perform a theoretical analysis and corresponding simulations, of the experimental signatures that can be expected in realistic scenarios by considering an X-ray laser pulse probing the quantum vacuum and interacting with an ultra-intense optical laser pump. Our results show that an ellipticity is induced in the polarisation of the probe laser, but also a rotation in the angle of polarisation. These results show the usefulness of the numerical tool developed in this work in complementing the community's current theoretical and experimental effort to detect the quantum vacuum.

Keywords: QED polarization, Maxwell solver, Finite Difference Time Domain

1. Introduction

The prospects offered by ultra-intense laser sources (in the infra-red (IR) or x-ray central wavelengths) have triggered a renewed interest in Quantum Electrodynamics (QED) and its impact on quantum processes at a macroscopic scale, namely how such phenomena can affect well studied interactions in the fields of plasma and laser dynamics. The most relevant QED processes in strong fields and high intensity laser interactions have been explored in several reviews [1, 2]. Among these effects, the second order QED process of photon-photon scattering mediated by the vacuum fluctuation of virtual electron-positron pairs has been a topic of renewed interest motivated by several exotic consequences [2] that originate directly from the original Heisenberg & Euler Lagrangian [3]. However, many of these effects, such as the virtual polarization of the vacuum, remain to be experimentally observed. With expected peak intensities up to $10^{23} - 10^{24}$ Wcm^{-2} to be delivered by large scale facilities such as the Extreme Light Infrastructure (ELI), the VULCAN 20 PW project, or the HERCULES laser upgrade, the regime where these virtual fluctuations can be detected is close to being within reach. In particular, experiments are being planned to study the quantum dynamics of the vacuum [4] by combining ultra-intense IR lasers with X-ray lasers. The increasing consensus regarding the importance of quantum dynamics in the collective effects of many extreme laser plasma systems has motivated the development of novel numerical tools that couple the multiple scales, ranging from plasma to quantum scales, associated with the problem. Numerical codes that simulate quantum radiation reaction [5] and pair production effects [6, 7], have already made important predictions in extreme energy density scenarios. However, a method to include the effect of vacuum polarization via the creation of virtual pairs, in multi-dimensions and for a broad set of initial conditions, has not been proposed yet. As further shown in this work, these vacuum quantum effects can be modelled as an effective nonlinear permeability and permittivity of the vacuum allowing us to adopt a semi-classical approach. The effects of the quantum vacuum can be important not only in scenarios involving high intensity electromagnetic radiation but also in the description of the formation and dynamics of the magnetosphere of pulsars [8].

The goal of this thesis was to develop a numerical

method that can self-consistently solve the resulting set of equations, when vacuum polarization effects are included within a semi-classical theory. The theoretical framework adopted will be presented in the next section and result in corrections to the classical set of Maxwell's equations with a nonlinear polarization and magnetization of the vacuum.

2. Theoretical framework

The electron-positron pair vacuum fluctuations were first taken into account by Heisenberg and Euler (HE) who calculated the first full corrected Lagrangian to all orders. In the low field $E \ll E_{Sch}$, low frequency $\omega \ll \omega_c$ limit of the electromagnetic (EM) fields, the leading corrections of the standard Maxwell Lagrangian density [3] can be written as

$$\mathcal{L} = \varepsilon_0 \mathcal{F} + \xi(4\mathcal{F}^2 + 7\mathcal{G}^2), \tag{1}$$

where the Compton frequency is given by $\omega_c = m_e c^2/\hbar$, the Schwinger critical field $E_{Sch} = m_e^2 c^3/e\hbar$ and the EM invariants $\mathcal{F} = E^2 - c^2B^2$ and $\mathcal{G} = \vec{E}\cdot\vec{B}$. The nonlinearities coupling parameter is

$$\xi = \frac{20\alpha^2\varepsilon_0^2\hbar^3}{45 m_e^4 c^5} \sim 10^{-51}\ [\mathrm{Fm/V^2}]\,. \tag{2}$$

This parameter weighs the relative importance of the quantum corrections compared to the classical fields and vanishes in the limit $\hbar \to 0$. Calculating the Euler-Lagrange equations for the electromagnetic fields, we obtain a set of modified Maxwell equations [9]

$$\vec{\nabla}\cdot\vec{D} = 0 \tag{3a}$$

$$\vec{\nabla}\cdot\vec{B} = 0 \tag{3b}$$

$$\vec{\nabla}\times\vec{H} - \frac{\partial\vec{D}}{\partial t} = 0 \tag{3c}$$

$$\frac{\partial\vec{B}}{\partial t} + \vec{\nabla}\times\vec{E} = 0\,, \tag{3d}$$

with

$$\vec{D} = \epsilon_0\vec{E} + \vec{P} \tag{4a}$$

$$\vec{B} = \mu_0\vec{H} + \vec{M}\,. \tag{4b}$$

In this approach, the effect of the quantum dynamics, arising from vacuum fluctuations modifies Ampère's law by a nonlinear vacuum polarization, $\vec{P}$, and magnetization, $\vec{M}$, given by

$$\vec{P} = 2\xi\left[2(E^2 - c^2B^2)\vec{E} + 7c^2(\vec{E}\cdot\vec{B})\vec{B}\right] \tag{5}$$

$$\vec{M} = -2\xi\left[c^2(2(E^2 - c^2B^2)\vec{B} - 7(\vec{E}\cdot\vec{B})\vec{E}\right]. \tag{6}$$

This semi-classical formulation effectively treats the vacuum as a nonlinear medium, being relevant when the EM invariants are non zero. In this work, we present an algorithm to solve the nonlinear set of corrected Maxwell's equations in a self-consistent manner. In the next section we will present the numerical algorithm developed to solve the set of eqs.(3c-3d) with the constitutive relations characterized by eqs.(5-6), that describe the behaviour of the quantum vacuum in the high intensity fields limit.

3. Numerical Algorithm

A standard finite-difference time domain (FDTD) method to solve Maxwell's equations is the Yee Algorithm [10]. The Yee scheme solves simultaneously for both electric and magnetic fields by solving Faraday's and Ampère's law, respectively. The explicit linear dependence of Maxwell's equations on the fields allows the field solver to be centered both in space and time (leap frog scheme), thus providing a robust, second order accurate scheme without the need to solve for simultaneous equations or matrix inversion [11]. Moreover, the efficiency and simplicity of the Yee scheme allow an easy incorporation into numerically parallel PIC codes. To solve the QED Maxwell equations, a modified Yee scheme was developed to address the difficulties which arise from the nonlinear polarization and magnetization terms. The nonlinear corrections to Ampère's law prevents each electric field component to be advanced in a straightforward manner as it requires the knowledge of future quantities The scheme proposed to overcome this difficulty is illustrated in Fig.1 for a time step Δt and now described:

- we begin by advancing the fields using the standard Yee scheme (i.e. without accounting for the polarization and magnetization of the vacuum). This setup allows us to obtain predicted quantities for the values of the fields at the new time. This approach is based on the standard technique of the predictor-corrector method, where the linear Maxwell equations are solved as the zeroth order solution to the fields;
- the predicted field values are then interpolated at all spatial grid points using a cubic spline interpolation method thus allowing to calculate quantities such as the EM invariants and respective polarization and magnetization of the vacuum, to lowest order;

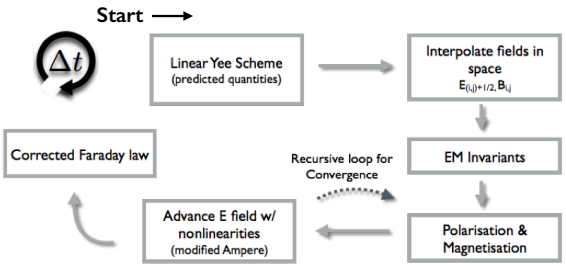

Figure 1: Full loop of the modified Yee scheme

– the polarization and magnetization are then used to advance the electric field via the modified Ampère's law;

– the convergence loop re-injects this new electric field value back into the polarization and magnetization source terms to refine these quantities and re-calculate the electric field iteratively. This loop is reiterated until the electric converges to a value within the desired accuracy;

– after convergence is achieved, Faraday's law is advanced, identically to the linear Yee scheme, benefiting from the fact that the electric field values being used are self-consistent with the QED corrections.

It must be emphasized that this method is only valid as long as the effects of the polarization and magnetization of the medium are small compared to the non-perturbed propagation of the fields given as solutions to Maxwell's equations in classical vacuum. This condition is automatically satisfied for realistic values of electromagnetic fields available in current, or near future, technology. In this regime, the QED theory is valid since the Schwinger field, above which the production of real electron-positron pairs is possible, corresponds to an electric field of $E_s \sim 10^{18}$V/m, whereas ambitious laser facilities aim to push available intensities to the $10^{23} - 10^{24}$ W/cm^2 ($E \sim 10^{15}$V/m) range. The order of the ξ parameter in eqs.(2,5,6) clearly helps to ensure the validity of the method. The convergence loop can be seen as a Born-like series since for every re-insertion of the fields back into the nonlinear source term, there is a gain in accuracy of one order in the expansion parameter to the result. This generalization of the Yee scheme can be extended beyond the framework of QED corrections to the vacuum as it is valid to solve Maxwell's equations in any nonlinear medium provided that the polarization and magnetization are given and that their order is such that they can be treated as a perturbation. This possible generalization enhances the range of applicability of our algorithm.

4. 1D Results

A thorough benchmark of the functionality and robustness of the algorithm may only be gained by comparing simulation results with analytical results in 1D simplified cases. The two cases we exploit here are the vacuum birefringence in the presence of a strong static field and counter propagating plane waves. Whilst the first case is well studied in the literature [12, 13], the second case requires a finer analytical work, yielding nevertheless the well known result of generation of higher harmonics due to the nonlinear interaction as shown in [14] in different setups and physical regimes. Finally, in all the results presented in this section, the units were normalized to the characteristic laser frequency, ω_0 and wave number, k_0. The normalizations are thus $t \to \omega_0 t$ and $x \to k_0 x$. These normalizations of space and time define the normalizations used for the fields, i.e: $E \to eE/mc\omega_0$ and $B \to eB/mc\omega_0$.

4.1. Vacuum Birefringence

The optical property of a change in refractive index of a material according to the polarization and propagation direction of the incoming light is called birefringence. If the optical medium in question is the vacuum, then this effect is refered to as vacuum birefringence. The birefringence of the vacuum is a thoroughly studied setup of great experimental interest to explore the properties of the quantum vacuum [15]. A one dimensional wave packet traveling in the presence of a strong static field will experience a modified refractive index of the vacuum due to the HE corrections. As first presented in [12, 13] and re-derived in our work, in the presence of a strong background electric field E_s, an electromagnetic pulse E_p, will experience one of the following refractive indexes:

$$n_{\parallel} = \left(\frac{1+6\xi E_s^2}{1+2\xi E_s^2}\right)^{1/2}, \quad (7)$$

$$n_{\perp} = \left(\frac{1+2\xi E_s^2}{1-5\xi E_s^2}\right)^{1/2}, \quad (8)$$

where the parallel and perpendicular directions refer to the direction of the probe polarization when compared to the static field. Notice that the product ξE_s^2 appears as a relevant quantity. This is a recurring property of several setups. It must be ensured that this product is a small quantity, both for the validity of the theoretical framework but also from the algorithm point of view.

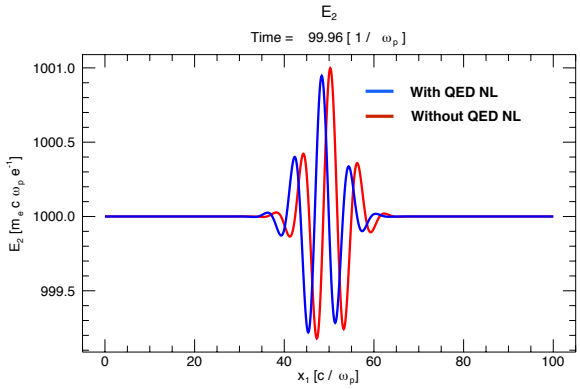

Figure 2: 1D Gaussian pulse after an entire propagation over a periodic box in the presence of a strong static field, with (blue) and without (red) QED nonlinearities

The simulation setup to test this theory consists of a strong static electric field of $10^{-3}E_{Sch}$ aligned along the y direction and a Gaussian EM pulse propagating in the x direction and polarized in the $y-z$ plane. The central wavelength of the EM Gaussian pulse is 1 μm and its duration 5.6 fs. Figure 2 shows two simulations for the same pulse after propagating once through a periodic box. In one case the propagation is in the classical vacuum, whereas the QED solver is used in the other. Qualitatively, the difference in propagation distance and the reduced electric field amplitude is consistent with the theory of a pulse traveling in a refractive medium. To test the accuracy of the algorithm this same setup was run for different values of the product ξE_s^2 for both the parallel and perpendicular setup. The difference in phase velocity between the two pulses allows to extract directly the quantum vacuum refractive indexes and to compare with the analytical predictions of eq.(7)-eq.(8). The results are shown in Fig. 3(a) and Fig.3(b) where an excellent agreement between simulation and theory is found. This 1D setup is useful, since the strong static field could model the electric field of another pulse with a much smaller frequency (static approximation).

4.2. *Counter-propagating plane waves*

As a second example, we considered a 1D periodic box with two counter-propagating plane waves polarized in the y direction, with the same frequency and amplitude. This interaction, which would normally result in a standing wave, is modified in the presence of the HE nonlinearities. This example also serves as an ideal benchmark for the accuracy and stability of the code, provided an exact analytic result can be obtained. The theoretical analysis to address this scenario is similar to

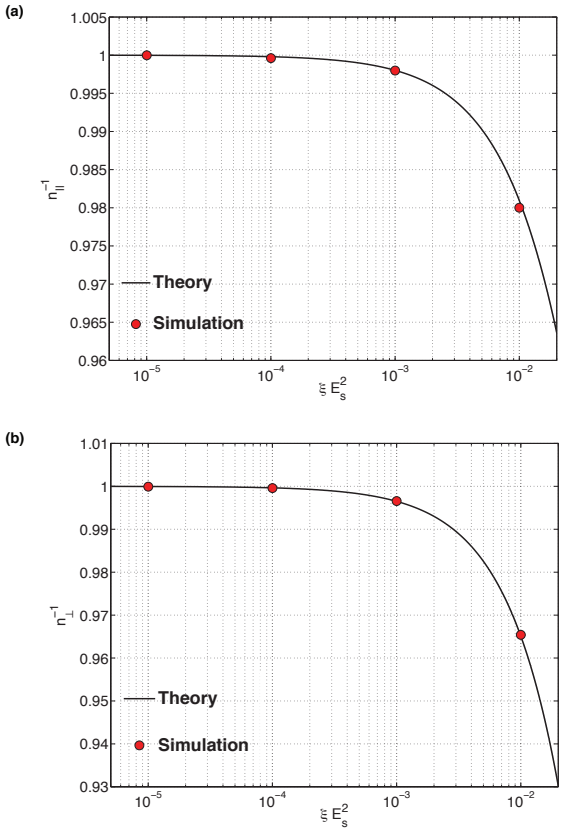

Figure 3: (a) Phase velocity ($c = 1$) of probe pulse with polarization parallel to E_s, (b) Phase velocity ($c = 1$) of probe pulse with polarization perpendicular to E_s, both as a function of ξE_s^2 parameter

a Born series of partial waves. Assuming that the solution of the QED Maxwell's equations are of the type

$$E = E_{(0)} + E_{(1)} + E_{(2)} + ... \quad (9)$$

$$B = B_{(0)} + B_{(1)} + B_{(2)} + ... \ , \quad (10)$$

where $E_{(0)}$ and $B_{(0)}$ are the unperturbed standing wave fields given by $E_{(0)} = E_0\,[\cos(x-t) + \cos(x+t)]$ and $B_{(0)} = B_0\,[\cos(x+t) - \cos(x-t)]$ whilst the remaining terms are successively higher order corrections to the standing wave fields, weighted by an expansion parameter to be identified. Starting from the modified Maxwell's equations and inserting eq.(9) and eq.(10) as the expressions for the fields, we arrive at the wave equation for the first order correction to the electric field $E_{(1)}$

$$\Box\, E_1 = S_1(x,t), \quad (11)$$

where $\Box$ is the d'Alembert operator and the source term $S_1 = -\partial_t\partial_x M + \partial_t^2 P$. Inserting in the source term, the

zero order field, i.e. $P, M = f(E_{(0)}, B_{(0)})$, we arrive at

$$S_{(1)}(x,t) = 16\xi E_0^3 \cos(t)\cos(x)\left[3\cos(2t) - \cos(2x)\right] \tag{12}$$

This source term only accounts for the unperturbed fields being inserted into the nonlinear polarization and magnetization. The formal solution of this equation is given by the convolution between the source term and the Green's function of the one dimensional wave operator, Performing this operation yields the modified electric field which reads

$$E_{(1)}(x,t) = -2\xi E_0^3 \sin(t)\cos(x)\left[2\sin(2t)\left(\cos(2x) - 2\right) - 4t\right]. \tag{13}$$

The corrected field exhibits a secular growth term modulated by an oscillating term. We also notice that the relative amplitude between this term and the unperturbed field amplitude is ξE_0^2 showing again that this perturbative treatment is valid as long as $\xi E_0^2 \ll 1$. Taking the spatial Fourier transform of $E_{(1)}$, we verify that the fundamental mode $\mathrm{k} = \mathrm{k}_0$ is reinforced by the linearly growing term and the appearance of an harmonic at $\mathrm{k} = 3\mathrm{k}_0$. Defining the Fourier transform of $E(x,t)$ as $\tilde{E}(k,t)$, we obtain

$$\tilde{E}_{(1)}(\mathrm{k} = \mathrm{k}_0) = 4\xi E_0^3 t \sin(t) + 3\xi E_0^3 \sin(t)\sin(2t), \tag{14}$$

$$\tilde{E}_{(1)}(\mathrm{k} = 3\mathrm{k}_0) = -\xi E_0^3 \sin(t)\sin(2t). \tag{15}$$

Repeating this process to higher orders, we can show that this nonlinear interaction generates odd higher harmonics from vacuum with the relative amplitude between these harmonics obeying the ordering

$$\tilde{E}(\mathrm{k} = 2n+1) = (\xi E_0^2)^n \tilde{E}(\mathrm{k} = \mathrm{k}_0) \tag{16}$$

These predictions were compared with the results of the QED solver using field amplitude of $E_0 = 0.025 E_{Sch}$, $\lambda_0 = 1\ \mu$m plane waves and $\xi = 10^{-9}$, such that the higher harmonics can be accurately resolved above the numerical noise.

We compared the simulation results with our model, by tracking the temporal evolution of the amplitude of the $\mathrm{k} = \mathrm{k}_0$ mode in Fourier space and comparing with eq.(14). Figure 4 shows the temporal evolution of $E_1(\mathrm{k} = \mathrm{k}_0)$. The simulation show an excellent agreement with the theoretical predictions for many laser cycles, ensuring that the algorithm is robust.

5. 2D Results

In order to illustrate this algorithm in multi-dimensions, two complex setups were investigated in

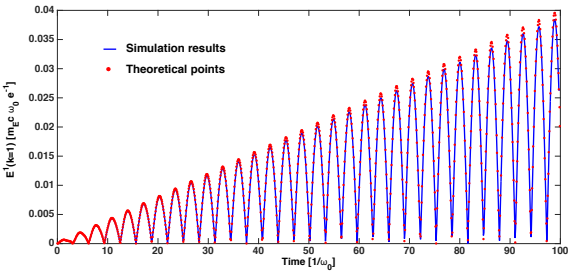

Figure 4: Temporal evolution of $\mathrm{k} = \mathrm{k}_0$ Fourier mode of the subtracted electric field

2D: the counter propagation of two Gaussian pulses interacting at the focal point, and the perpendicular interaction of two Gaussian pulses focused at the same point. For these setups, a consistent analytical treatment becomes cumbersome especially due to the self-consistent treatment of both the transverse and longitudinal component of the pulses. A quantum parameter of $\xi = 10^{-6}$ was used for the sake of providing illustrative examples. In the first setup two $\lambda = 1\mu$m laser beams with a normalized vector potential $\mathrm{a}_0 = 50$ ($\sim 10^{-4} E_{Sch}$ in normalized units) and duration of 25 femtoseconds were counter-propagated and interacted in the presence of the QED nonlinearities. Both beams had a waist $\mathrm{W}_0 = 2.3\mu$m. Fig.5-(a) shows the spatial Fourier transform of the beams with $\xi = 0$ (classical limit) and in Fig. 5-(b) the Fourier transform of the electric field after the interaction (asymptotic state) including the HE corrections. As shown in Fig. 5-(b), after the interaction odd higher harmonics are also generated as in the 1D case, with relative amplitudes consistent with eq.(16). However, in this case the harmonics generated have the same Gaussian behavior as the unperturbed pulses and attain a greater spread in Fourier space after the interaction. After the pulses have spatially overlapped, the harmonics propagate and leave an imprint of the nonlinear interaction, that co-propagates with the original beam. The second setup is more rich: it comprises of two 1μm Gaussian pulses propagating in perpendicular directions with $\mathrm{a}_0 = 50$ that interact at their focus. The beam parameters are equal to those of the previous setup. The initial Fourier space of the beam propagating in the x direction is shown in Fig. 6-(a) and this spectrum would remain unaltered during the interaction in the classical limit ($\xi = 0$). During the peak of the nonlinear interaction (at the focal point) we see in Fig. 6-(b) that many pairs of $(\mathrm{k}_1, \mathrm{k}_2)$ harmonic combinations are being generated. More interestingly, there appears to be a continuous filling of Fourier space in between

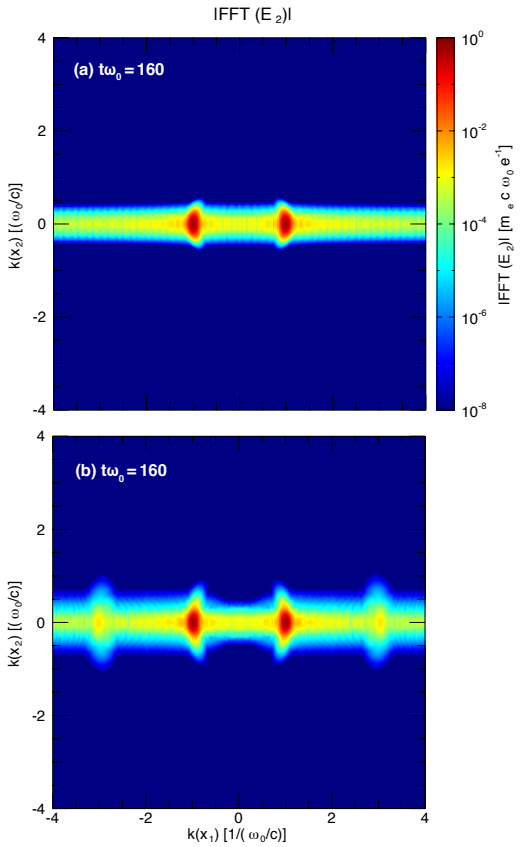

Figure 5: Spatial Fourier transform of the electric field, (a) after the interaction but when QED corrections are absent, (b) after the interaction with self-consistent inclusion of the quantum corrections. $k = 3k_0$ harmonics and small distortion of $k = k_0$ can be observed.

the expected harmonics integer combination as the spatial overlap creates a multitude of nonlinear Gaussian modes. This effect is then lessened after the interaction has occurred since there is no longer a source to feed these regions of Fourier space and only the integer expected combination of (k_1, k_2) harmonics are left as an imprint of the interaction, see Fig. 6-(c). The longitudinal field component triggers a self-interaction of the Gaussian pulse through the QED nonlinearities. This self-interaction plays the role of a coupling source when both pulses interact spatially. The Fourier spectra obtained in these two setups show that the harmonics generated in either case are distinct, thus allowing to clearly distinguish both cases. Namely, it is of great interest to understand how the production of these higher harmonics from vacuum may be optimized in terms of the duration of the pulses as these results can provide signatures of experimental relevance. A future setup to explore will also include the interaction of two laser beams at

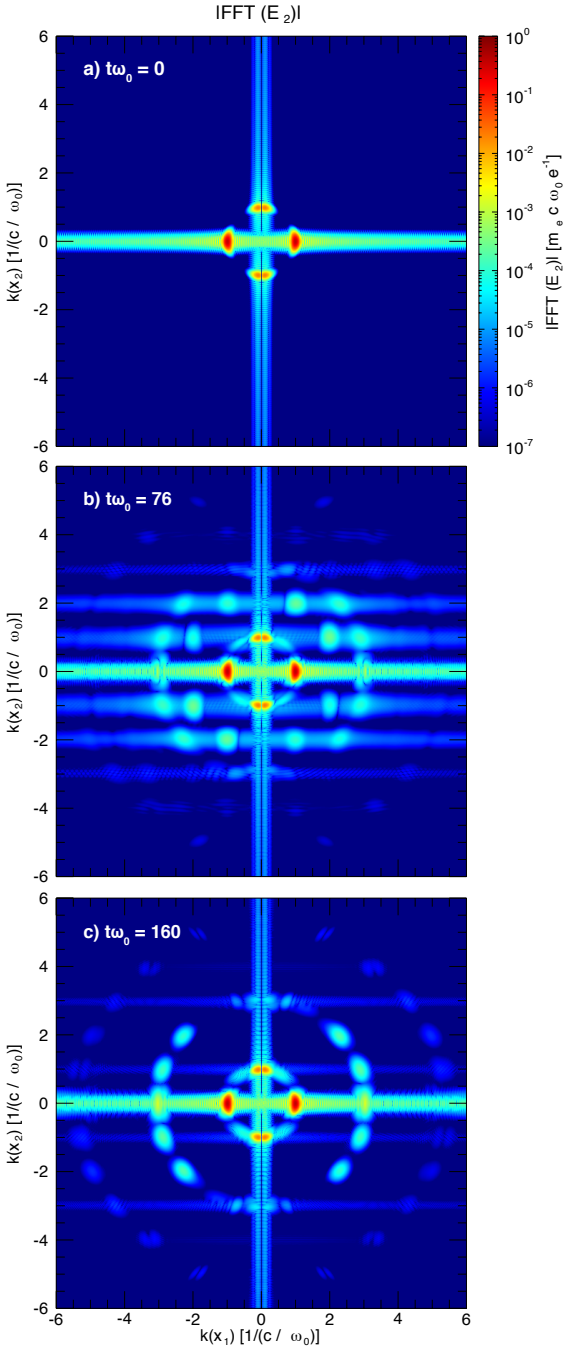

Figure 6: Spatial Fourier transform for E_2 field at different stages of interaction. (a) Initial Fourier space (b) At peak of nonlinear interaction when the pulses are overlapped in space. (c) Asymptotic state: after the nonlinear interaction the pulses propagate independently but with higher harmonics generated from the interaction.

an arbitrary angle $0 < \theta < \frac{\pi}{2}$ radians in order to model realistic experimental conditions. If this angular dependence of the interaction is well understood, one could in principle determine how well aligned two ultra-intense beams are by looking at the Fourier spectrum after a vacuum interaction. Finally, if one assumes that the parameter ξ is a well measured quantity, one could precisely measure the initial intensity of the beams.

6. Realistic scenarios of vacuum birefringence

6.1. Theoretical model and setup

In the final section of the work we start by explaining the experimental setup proposed for the measurement of vacuum birefringence followed by an extension of the theoretical analysis performed for the birefringence of the vacuum. We show that the physical observables in realistic setups are the ellipticity and angle of rotation in the polarization of a probe pulse. We show show that realistic simulations can be performed using the new numerical solver developed in this thesis, whilst emphasizing the fact that such is only possible using high performance computing tools. As originally proposed in [13, 12] an X-ray probe pulse of wavelength λ_X will experience vacuum birefringence when counter-propagated with a strong optical pump laser of wavelength λ_0. In particular, due to the difference of scales ($\lambda_X \ll \lambda_0$), the X-ray probe will effectively experience a quasi-static field according to the pump profile. The setup of interest is illustrated in fig.7 where we see the X-ray probe pulse initially polarized at 45 compared to the polarization of the pump pulse, leaving the region of interaction with an ellipticity induced in its polarization as well as a rotation on the plane of polarization, due to the quantum vacuum interaction. To address the

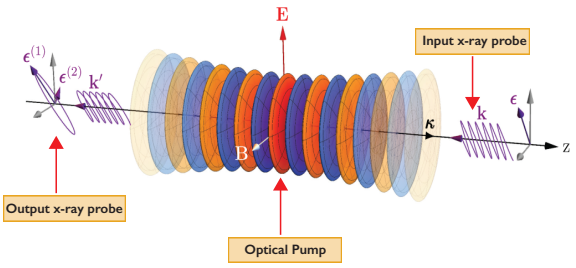

Figure 7: Experimental setup proposed to study the birefringence of the quantum vacuum via the change in the ellipticity of the polarization of a X-ray probe pulse, after trasversing a strong optical pump laser.

setup proposed, we simulate the following 2D setup, in a 1D limit, with all beams initialised as plane waves in the transverse direction. The setup comprises of a 10 keV X-ray that is counter-propagated with a 1 μm optical pulse, both with duration of 40 fs. The intensity of the optical pump is 10^{23} Wcm^{-2} whereas the X-ray laser had an intensity of 10^{18}Wcm^{-3}. These parameters were chosen according to the proposed beam parameters for the LCLSII update and the new SLAC X-ray laser.

The theoretical analysis was performed as follows. A laser probe with EM fields $\vec{E_p}, \vec{B_p}$ was counter-propagated with a laser pump of EM fields $\vec{E_0}, \vec{B_0}$, and the relative polarization between both lasers taken to be a general angle θ that was then set to $\frac{\pi}{4}$, in order to maximize the effects of the Quantum vacuum. We then performed a perturbative calculation, detailed in the thesis, where the unperturbed pump field and the unkown self-consistent probe, were inserted in the nonlinear polarization and magnetization of the vacuum. Applying an ordering to the resulting equations, allows us to obtain a wave-equation for the probe pulse and a corresponding dispersion relation in the limit of a slowly varying pump profile. To make the calculations feasible, we assume that the pump laser is unaffected by the nonlinear interaction with the probe laser. Applying the ansatz we obtain the following dispersion relation for the component of the probe pulse parallel to the pump laser field,

$$a_{\parallel}\omega^2 + \omega(j\gamma_{\parallel} - \beta_{\parallel}k) - (k^2 b_{\parallel} + \alpha_{\parallel} - j\gamma_{\parallel}k) = 0\,. \quad (17)$$

Where the coeficients are defined as

$$\begin{aligned} \alpha_{\parallel} &= 8\xi(\partial_t\partial_x E_0^2 - \partial_t^2 E_0^2)\,, \\ \gamma_{\parallel} &= 4\xi(\partial_x E_0^2 - 3\partial_t E_0^2)\,, \\ \beta_{\parallel} &= 8\xi E_0^2\,, \\ a_{\parallel} &= 1 + 4\xi E_0^2\,, \\ b_{\parallel} &= 1 - 4\xi E_0^2\,. \end{aligned}$$

Note that despite the coefficients having spatial and temporal dependence, due to the pump laser profile, they vary on a larger scale compared to the characteristic frequency and wavelengths of the probe pulse which permits to approximate these coefficients as quasi static and apply the WKB approximation. The dispersion relation is quadratic in ω and can therefore be solved using the quadratic formula to yield two roots. Applying the quadratic formula to Eq.(17) yields,

$$\omega = \frac{\beta_{\parallel}k - j\gamma_{\parallel} \pm \sqrt{(j\gamma_{\parallel} - k\beta_{\parallel})^2 - 4a_{\parallel}(jk\gamma_{\parallel} - b_{\parallel}k^2 - \alpha_{\parallel})}}{2a_{\parallel}}\,. \quad (18)$$

From Eq.(18), we confirm that a imaginary component arises in the dispersion relation, from the first term proportional to $\gamma_{\parallel}$ and also from the square-root which

is a complex number. This imaginary component in the dispersion relation means that the solution to Eq.(17) will be complex, with an imaginary component that will lead to an exponential growth or damping of the probe amplitude in time.

This expression can be simplified by replacing the spatial and temporal derivatives of the pump pulse by the characteristic scale of variation, $1/\sigma$ where σ is the duration of the pump laser. This process finally yields the following expression for the real and imaginary parts of the dispersion relation,

$$\omega = \omega_r + j\omega_i \,, \tag{19}$$

$$\omega_r \approx k\left(\sqrt{\frac{b_\parallel}{a_\parallel}} - \frac{\beta_\parallel}{2a_\parallel}\right), \tag{20}$$

$$\omega_i \approx \frac{\gamma_\parallel}{2a_\parallel}\left(1 + \sqrt{\frac{a_\parallel}{b_\parallel}}\right). \tag{21}$$

Equations (19-21), completely describe the propagation of the parallel component of the probe pulse. The same calculation was repeated for the component of the probe perpendicular to the pump laser yielding equations exactly in the same form but with the coefficients changed to,

$$\begin{aligned}
\alpha_\perp &= 14\xi(\partial_t\partial_x E_0^2 - \partial_t^2 E_0^2),\\
\gamma_\perp &= 7\xi(\partial_x E_0^2 - 3\partial_t E_0^2),\\
\beta_\perp &= 14\xi E_0^2,\\
a_\perp &= 1 + 7\xi E_0^2,\\
b_\perp &= 1 - 7\xi E_0^2 \,.
\end{aligned}$$

A crucial conclusion of this analysis is the fact that both the real part and imaginary part of the dispersion relation for the parallel and perpendicular components are different. This means that the phase velocity of each component will be different and thus an ellipticity will be induced in the polarisation as already discussed previously.

Furthermore, we have shown that there is a damping in the amplitude of the probe pulse due to the space-time variation of the pump laser during the nonlinear interaction. The fact that the damping factor is different for both the parallel and perpendicular components means that after the interaction, they will no longer have the same amplitude. This mismatch in the amplitude of both components, small as it may be, will induce a rotation in the polarization angle of the probe pulse. Finally, the fact that the damping rate does not depend on the probe wave-number but rather only on the characteristics of the pump, is a valuable conclusion. As already emphasized, this setup of great experimental relevance, can be simulated with the algorithm developed in our work. In the next section we will analyse the results of the simulations performed and compare with our theoretical predictions in both a quantitative an qualitative manner.

6.2. Simulation result analysis

A crucial feature present in the simulations performed is the difference in scales between the two laser pulses. This difference in scales (optical to X-ray) is about 3 orders of magnitude. Furthermore, the simulation parameters had to be such that the wavelength of the X-ray probe could be resolved with a criteria of 20 points per wavelength but also the width of the wave packages must be captured within the simulation domain. These restrictions bring us to a crucial point of this work: the fact that large computational resources are necessary to perform such simulations and that the algorithm must be fully paralelized to operate on large computing clusters.The simulations about to be presented were performed at the ACCELERATES cluster (Lisbon, Portugal). The fact that the algorithm we implemented was done in a fully parallel way represents a significant competitive advantage. Regarding the value of the quantum coupling parameter ξ, we chose to vary this parameter whilst maintaining the remaining simulation parameters constant. The one-dimensional theory previously presented can be applied to the simulation setup as we used plane waves in the transverse direction for both probe and pump. However, the longitudinal profile of both pulses can be intialised with any function desired. In particular, it is of interest to test how the results vary according to the wave packet of the pump laser. To understand this dependence, we performed simulations for different values of ξ parameters but also for two different functions for the pump laser profile:

$$E_0(x, t=0) = E_0 \exp\left(\frac{-(x-x0)^2}{2\sigma^2}\right), \tag{22}$$

$$E_0(x, t=0) = E_0 \cos(k_0 x) \exp\left(\frac{-(x-x0)^2}{2\sigma^2}\right). \tag{23}$$

Where k_0 and σ are the wave-number and duration of the pulse, respectively. These profiles were selected to compare the induced ellipticity and rotation of polarisation when the pump laser is a Gaussian package to when that same package is modulated by an oscillating function. Most importantly, whilst eq.(23) has associated to it two spatial scales (σ, k_0), the profile in eq.(22) only has one scale of variation. Furthermore, the spatial integral over the square of the pump profile is an

important quantity that measures the effective length of interaction between the probe pulse and the birefringent medium. In the thesis we show that this integral differs by a factor of both two when performed over eq.(22) or eq.(23).

This difference corresponds to the existence of multiple wavelengths within the pump envelope leading us to expect the results of the simulations for both cases, in terms of the ellipticity induced and rotation of polarisation, to differ by a factor of approximately two. The resulting ellipticity induced in the polarization was calculated for each type of pump profile yielding

$$\delta_{\text{theo1}} = \frac{3}{2} k_0 \sqrt{\pi}\sigma\xi E_0^2 \,, \tag{24}$$

$$\delta_{\text{theo2}} = 3k_0 \sqrt{\pi}\sigma\xi E_0^2 \,. \tag{25}$$

Where the 1,2 subscripts refer to each pump profile, Eqs.(22-23), respectively. In this calculation the real part of the dispersion relation was approximated by Eq.(20). We developed an ellipticity diagnostic that computed the minor radius, b_{sim} of the ellipse induced in the polarization of the probe pulse. This value can be related to the ellipticity induced in the polarization by

$$\delta_{\text{sim}} = \frac{2\sqrt{2}}{E_p} b_{\text{sim}} \,. \tag{26}$$

This result can then be compared to the theoretical expressions, Eqs.(24-25). Having derived theoretical expressions for the ellipticity expected from the simulation, using the real part of the dispersion relation, we also derived the corresponding theoretical angle of rotation. This was done by estimating the imaginary part of the dispersion relation thus arriving at the expected damping rate of each component given by

$$\Gamma_{\parallel 1} \approx 4\xi E_0^2\sigma, \tag{27}$$

$$\Gamma_{\perp 1} \approx 7\xi E_0^2\sigma, \tag{28}$$

$$\Gamma_{\parallel 2} \approx 8\xi E_0^2\sigma, \tag{29}$$

$$\Gamma_{\perp 2} \approx 14\xi E_0^2\sigma \,. \tag{30}$$

Where again, the 1,2 subscripts refer to each pump profile. We show that the angle of rotation of polarisation can be theoretically calculated using the damping rates computed. These expressions, for each case of the pump profile, are given by,

$$\Delta\phi_{\text{theo1}} = \frac{\pi}{4} - \arctan\left(e^{-3\xi E_0^2\sigma}\right), \tag{31}$$

$$\Delta\phi_{\text{theo2}} = \frac{\pi}{4} - \arctan\left(e^{-6\xi E_0^2\sigma}\right), \tag{32}$$

The simulation described was repeated for different values of ξ. The ellipticities induced and the polarisaion rotation angles were extracted from the simulation and are plotted in fig.8(a)-(b). The same plot also includes the corresponding theoretical expressions eqs(24-25) and eqs.(31-32), respectively. The first conclusion that can be drawn from the results in fig.8(a)-(b) is that the simulation points both for the ellipticity induced and also for the polarisation rotation angle, change by a factor of 2 when comparing the results with each type of pump profile. This result is in remarkable agreement with what we had predicted and seems to indicate that the shape of the longitudinal profile of the pump can be taken into account using our technique. On the other hand, for both physical quantities, the theoretical expressions previously derived and plotted as the orange and blue lines show a good agreement with the simulation results up

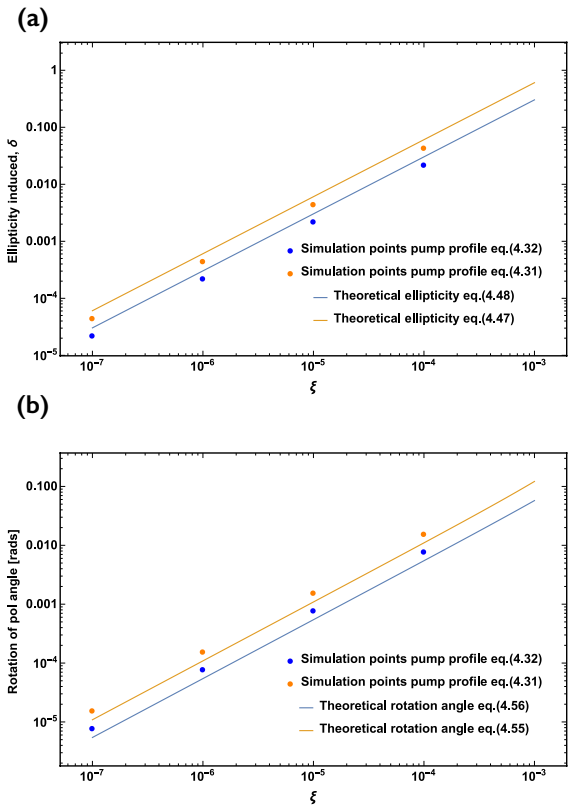

Figure 8: Figure comparing the quantities extracted from the simulations performed for different values of the quantum coupling parameter. (a) Ellipticity induced: the points in blue and orange refer to the results of the simulations using eqs.(23),22), compared to the theoretical expressions eqs.(25,24), respectively. (b) Polarization angle: The points in blue and orange refer to the results of the simulations using eqs.(23),22), compared to the theoretical eqs.(32,31), respectively.

to a multiplicative factor of the order of unity. Despite the agreement between theory and simulation not being perfect, we were able to derive useful expressions and above all, show that the algorithm is able to reproduce all the physical effects that we predicted, most importantly, we have shown that these physical effects scale linearly with the quantum parameter ξ of the simulation. This final conclusion if extremely valuable, as it shows that for future more complex simulations, it is reasonable to use an increased value of ξ, without changing the reliability and accuracy of the physical results obtained.

7. Conclusions

A numerically stable and robust generalized Yee scheme to solve the nonlinear set of QED Maxwell's equations was developed. This work represents an important step towards modeling plasma dynamics in extreme scenarios when QED processes significantly alter the collective behavior of the system. Furthermore, our work can be used to benchmark planned experiments, leveraging on ultra-intense laser facilities able to deliver intensities of 10^{23} – 10^{24} W/cm^2, to verify for the first time the dynamics of the quantum vacuum below the Schwinger limit. The simulations confirm predicted optical phenomena such as vacuum birefringence and high harmonics generation in one-dimensional setups with an excellent accuracy. The code was also extended for two-dimensional scenarios where two setups of interacting Gaussian beams were studied. The results highlight the importance of transverse beam effects and hint that the generation of higher harmonics from quantum vacuum can be achieved via this interaction. The spectrum of the harmonics could provide a direct measurement of important beam properties such as the peak intensity and alignment. This algorithm may also be used to test two and three dimensional setups that have been proposed in the literature (where transverse and finite spot size effects are taken into account under certain approximations), thus complementing the results of previous theoretical works [16, 17]. Furthermore, we have shown that our algorithm can be used to simulate setups of experimental interest aiming to detect the existence of the quantum vacuum by measuring changes in the ellipticity and angle of polarisation of a X-ray pulse probing a birefringent vacuum created by a strong pump. This final demonstration illustrates how the algorithm developed in this Master thesis can be a powerful tool for the strong field QED community by delivering simulation results in multi-dimensional EM setups that can complement the theoretical work being developed using other formalisms, to understand the quantum vacuum. Finally our algorithm contributes to the generalization of the Yee scheme, one of the most successful and commonly used algorithms in computational physics, to scenarios where nonlinear polarization and magnetization can impact EM propagation.

[1] A. Di Piazza, C. Müller, K. Z. Hatsagortsyan, and C. H. Keitel. Extremely high-intensity laser interactions with fundamental quantum systems. *Rev. Mod. Phys.*, 84:1177–1228, Aug 2012.

[2] Mattias Marklund and Padma K. Shukla. Nonlinear collective effects in photon-photon and photon-plasma interactions. *Rev. Mod. Phys.*, 78:591–640, May 2006.

[3] W. Heisenberg and H. Euler. Folgerungen aus der diracschen theorie des positrons. *Zeitschrift fr Physik*, 98(11-12):714–732, 1936.

[4] T. Heinzl and A. Ilderton. Exploring high-intensity qed at eli. *The European Physical Journal D*, 55(2):359–364, 2009.

[5] M. Vranic, Grismayer T., R. A. Fonseca, and L. O. Silva. Quantum radiation reaction in head-on laser-electron beam interaction. *ArXiv*, 1511.04406, 2015.

[6] Thomas Grismayer, Marija Vranic, Joana. L Martins, Ricardo Fonseca, and Silva Luis. O. Seeded qed cascades in counter propagating laser pulses. *ArXiv*, 1511.07503, 2015. submitted to Physical Review E.

[7] C. P. Ridgers, C. S. Brady, R. Duclous, J. G. Kirk, K. Bennett, T. D. Arber, and A. R. Bell. Dense electron-positron plasmas and bursts of gamma-rays from laser-generated quantum electrodynamic plasmasa). *Physics of Plasmas*, 20(5), 2013.

[8] J Pétri. A 3+ 1 formalism for quantum electrodynamical corrections to maxwell equations in general relativity. *Monthly Notices of the Royal Astronomical Society*, 451(4):3581–3586, 2015.

[9] Marin Soljačić and Mordechai Segev. Self-trapping of electromagnetic beams in vacuum supported by qed nonlinear effects. *Phys. Rev. A*, 62:043817, Sep 2000.

[10] Kane Yee. Numerical solution of initial boundary value problems involving maxwell's equations in isotropic media. *Antennas and Propagation, IEEE Transactions on*, 14(3):302–307, May 1966.

[11] Allen.Taflove and Susan C. Hagness. *Computational Electrodynamics*. Artech House; 3 edition (May 31, 2005), 2005.

[12] R. Baier and P. Breitenlohner. The vacuum refraction index in the presence of external fields. *Il Nuovo Cimento B (1971-1996)*, 47(1):117–120, 2015.

[13] E. Brezin and C. Itzykson. Polarization phenomena in vacuum nonlinear electrodynamics. *Phys. Rev. D*, 3:618–621, Jan 1971.

[14] B. King, P. Böhl, and H. Ruhl. Interaction of photons traversing a slowly varying electromagnetic background. *Phys. Rev. D*, 90:065018, Sep 2014.

[15] G. Zavattini, U. Gastaldi, R. Pengo, G. Ruoso, F. Della Valle, and E. Milotti. Measuring the magnetic birefringence of vacuum: The pvlas experiment. *International Journal of Modern Physics A*, 27(15):1260017, 2012.

[16] A. Di Piazza, K. Z. Hatsagortsyan, and C. H. Keitel. Light diffraction by a strong standing electromagnetic wave. *Phys. Rev. Lett.*, 97:083603, Aug 2006.

[17] Victor Dinu, Tom Heinzl, Anton Ilderton, Mattias Marklund, and Greger Torgrimsson. Photon polarization in light-by-light scattering: Finite size effects. *Phys. Rev. D*, 90:045025, Aug 2014.